ACS APPLIED MATERIALS & INTERFACES

Research Article

www.acsami.org

# Nanospot Soldering Polystyrene Nanoparticles with an Optical Fiber Probe Laser Irradiating a Metallic AFM Probe Based on the Near-Field Enhancement Effect

Jianlei Cui,[†,‡,§,∥] Lijun Yang,[§,∥] Yang Wang,[§,∥] Xuesong Mei,[*,†] Wenjun Wang,[†] and Chaojian Hou[§,∥]

[†]State Key Laboratory for Manufacturing Systems Engineering, Xi'an Jiaotong University, Xi'an 710049, PR China

[‡]State Key Laboratory of Surface Physics and Department of Physics, Fudan University, Shanghai 200433, PR China

[§]Key Laboratory of Micro-systems and Micro-structures Manufacturing, Ministry of Education and [∥]School of Mechatronics Engineering, Harbin Institute of Technology, Harbin 150001, PR China

Supporting Information

**ABSTRACT:** With the development of nanoscience and nanotechnology for the bottom-up nanofabrication of nanostructures formed from polystyrene nanoparticles, joining technology is an essential step in the manufacturing and assembly of nanodevices and nanostructures in order to provide mechanical integration and connection. To study the nanospot welding of polystyrene nanoparticles, we propose a new nanospot-soldering method using the near-field enhancement effect of a metallic atomic force microscope (AFM) probe tip that is irradiated by an optical fiber probe laser. On the basis of our theoretical analysis of the near-field enhancement effect, we set up an experimental system for nanospot soldering; this approach is carried out by using an optical fiber probe laser to irradiate the AFM probe tip to sinter the nanoparticles, providing a promising technical approach for the application of nanosoldering in nanoscience and nanotechnology.

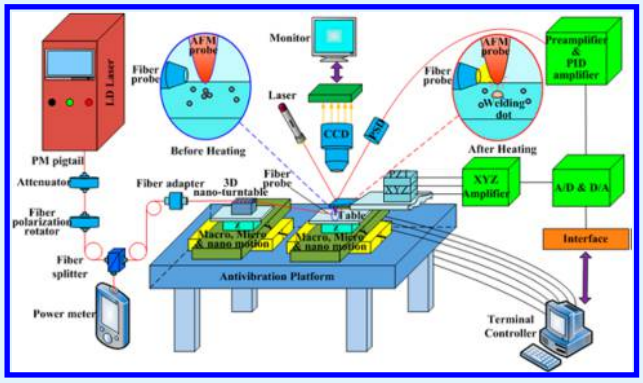


**KEYWORDS:** *nanospot soldering, polystyrene nanoparticles, near-field, AFM, optical fiber probe*

## 1. INTRODUCTION

With the development of nanoscience and nanotechnology, new nanomaterials, nanostructures, and nanofeatures are constantly discovered and fabricated, showing broad application prospects in the field of new materials, biomanufacturing, bionic manufacturing, hydrogen fuel cells, solar cells, information devices and equipment, and other high-performance scientific instruments. Although most of the focus has been on synthesizing carbon nanotubes, graphene, etc.,[1−3] structures created from polymers hold substantial promise. Because of the interesting properties of polymer particles with small size and high surface-to-volume ratios, polymer particles are used in the fabrication of nanoscale devices. Specifically, because polystyrene (PS) has been studied extensively and is readily available, it is gaining particular interest.[4−6] However, in the bottom-up nanofabrication of nanostructures formed from PS nanoparticles, joining technology is an essential step in the manufacturing and assembly of nanodevices and nanostructures in order to provide mechanical integration and connection.[7−9]

With regard to the PS nanoparticles being a promising candidate for nanostructure building blocks, the nanosoldering of adjacent PS particles has been demonstrated by thermal processing. Yi et al.[10] reported the sintering of 500 nm diameter PS nanoparticles on patterned substrates. Harel et al.[11] demonstrated the fabrication of PS nanostructure by nanomanipulation and thermal processing. However, during thermal processing, all of the PS particles in either the softening or the melting process were affected by the heated substrate, and the researchers could not achieve effective nanospot soldering of specified adjacent PS nanoparticles without affecting other PS particles.

On the basis of the application prospects and the soldering situation of PS nanoparticles described herein, we report for the first time a new nanospot-soldering method with an optical fiber probe laser irradiating a metallic AFM probe that is based on the near-field enhancement effect, and we demonstrate the effectiveness and feasibility of nanospot soldering from the theoretical and experimental viewpoints.

## 2. NEW IMPLEMENT FOR NANOSPOT SOLDERING

To achieve nanospot soldering with a laser, obtaining a nanospot light source with a sufficently high power becomes the key to success at eliminating the diffraction limit restriction.

Received: September 16, 2014
Revised: January 9, 2015
Accepted: January 13, 2015
Published: January 13, 2015





DOI: 10.1021/am506344j
ACS Appl. Mater. Interfaces 2015, 7, 2294−2300

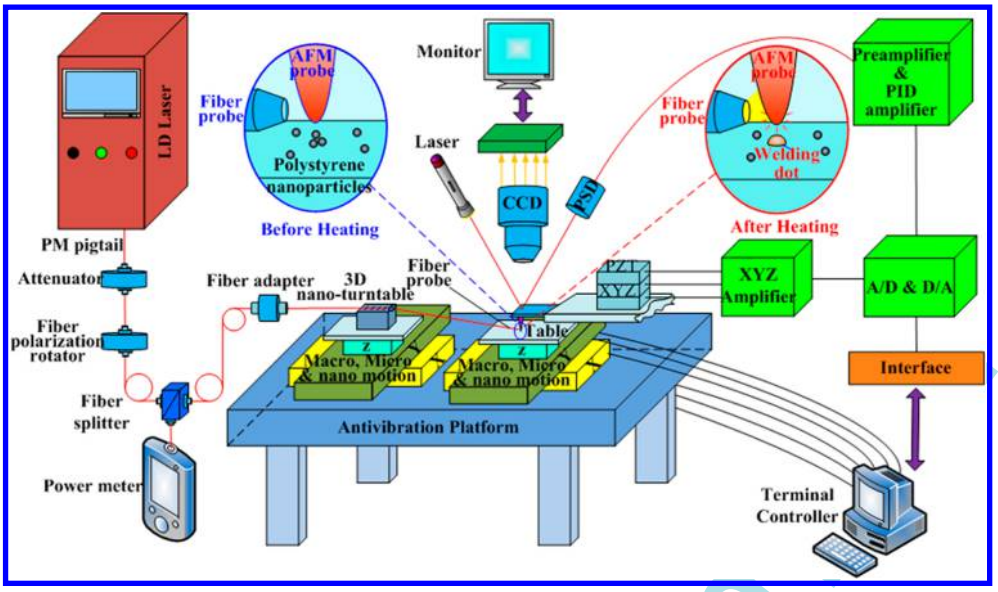


**Figure 1.** Schematic diagram of nanospot soldering of polystyrene nanoparticles with an optical fiber probe laser that irradiates the metallic AFM probe tip.

On the basis of the near-field optical theory,[12−15] if a micronano probe is irradiated by a strong focusing laser or a near-field laser, then an enhanced electromagnetic field with a very high field-enhancement factor will appear around the probe tip. Under laser irradiation, the free electrons in the micronano probe tip are in a collective oscillation. If the oscillation frequency of the electrons is consistent with the frequency of the incident laser, then resonance will be produced. In the resonant state, the energy of electromagnetic field can be effectively transformed into a collective oscillation energy of the free electrons of the micronano probe tip and the PS nanoparticles. The PS nanoparticles can melt and be joined together. At the same time, with the advent of the scanning tunneling microscope (STM) and the atomic force microscope (AFM) as tools for both imaging and micronano manipulation, nanospot soldering can be achieved; the new implement for nanospot soldering is illustrated in Figure 1.

In this system, the laser can be transmitted by the fiber and be focused by the optical fiber probe. The light that is reflected from the tapered, metallic probe tip is propagated to the optical fiber and is directed by the fiber splitter to a power meter for detection. A polarization rotator can be used to adjust the polarization direction of incident laser. This light is optimized to ensure that the laser beam is efficiently coupled into the core with a diameter of several micrometers and then directed all the way to the fiber tip. The combination of a flange attenuator and a polarization rotator permits both continuous variation of the laser power and polarization that are suited to the nanospot-soldering process. The optical fiber probe, placed in the guide unit to avoid vibration, is attached to a multidimensional nanopositioning stage and then is inserted into the sample object stage. As the optical system, the all-fiber-coupling optical circuit with low loss can match the optical probe as a result of good transmission. Therefore, the spatial light path is very flexible, and in the nanospot-soldering procedure, the relative position between the AFM probe tip and the optical fiber probe tip can be controlled by the multidimensional positioning stage with high accuracy, which is useful for subsequent nanospot-soldering procedures.

## 3. THEORETICAL ANALYSIS AND DISCUSSION

To study the near field of the metallic AFM probe tip as it is irradiated by the optical fiber probe laser, Figure 2 shows the corresponding computational model.

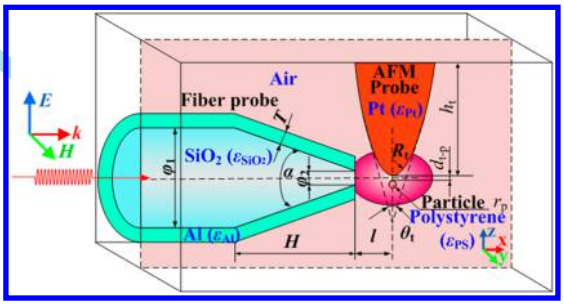


**Figure 2.** Computational model of the metallic AFM probe tip, irradiated by a tapered metal-coated optical-probe laser.

In the model, the incident laser transmits along the $x$-axis direction with the polarization direction along the $z$-axis direction. To ensure the accuracy and reliability of simulation results, the simulation model and parameters were as much as possible set to match the actual situation. On the basis of the actual parameters of optical fiber probe, the larger-end diameter of fiber probe $\varphi_1$, smaller-end diameter $\varphi_2$, and the length $H$ were set to ∼700, 100, and 600 nm, respectively. The curvature radius $R_t$ and the taper angle $\theta_t$ of the AFM probe tip (Si material coated with a Pt film) were set to 20 nm and 30°, respectively. According to the near-field excitation conditions necessary for the appearance of the near-field enhancement effect, the AFM probe was placed in the near-field region of optical fiber probe, and the distance $l$ was set to 70 nm in the corresponding simulations. Considering the actual laser instruments and the near-field enhancement effect, the laser wavelength was set to 808 nm. To calculate the enhancement characteristics at the corresponding laser wavelength, the relative permittivity values ($\varepsilon_{SiO_2}$ and $\varepsilon_{Al}$ for the optical fiber probe and $\varepsilon_{Si}$ and $\varepsilon_{Pt}$ for the AFM probe tip) were set to 3.9, −34.5 + $i$8.5, 13.6 + $i$0.044, and −17.179 + $i$29.609,


DOI: 10.1021/am506344j
ACS Appl. Mater. Interfaces 2015, 7, 2294−2300

respectively. In addition, the relative dielectric constant $\varepsilon_{PS}$ and the electrical conductivity of PS nanoparticles were set to 2.55 and 0.0167 S/m, respectively.[16] Because the penetration depth of the laser in aluminum material is very small in the actual situation of the optical fiber probe, the thickness of the aluminum film $T$ was set to 80 nm in order to limit the scattering and transmitting of light. At the same time, the metallic AFM probe tip and the PS nanoparticle were placed in the near-field region of optical fiber probe. To prevent the contamination of the AFM probe tip by PS nanoparticles, the distance $d_{t\text{-}p}$ between the AFM probe tip and the PS nanoparticle was set to 10 nm in the simulations. The diameter of the PS nanoparticle was set as 120 nm to obtain accurate data.

On the basis of the computational model, to analyze the near-field effect of the metallic AFM probe that was irradiated by an optical fiber probe laser, it was simulated with the finite element method, and the enhanced electric field is shown in Figure 3. For the purpose of clearly and simply expressing the

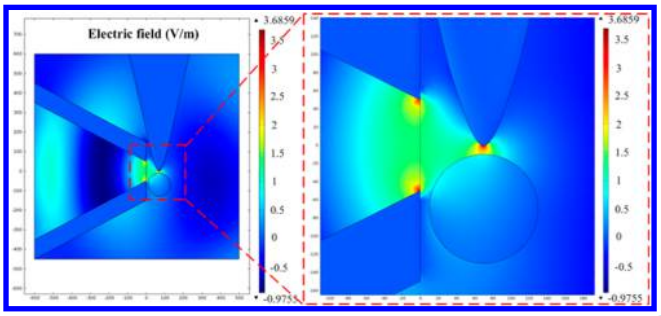


**Figure 3.** Electric field distribution with an optical-fiber-probe laser irradiating the metallic AFM probe and the polystyrene nanoparticle.

near-field enhancement effect, the electric field amplitude of the incident laser $E_0$ was set to 1 V/m. At the outlet portion of optical fiber probe, the strength of the electric field has a high value attributable to the near-field enhancement effect that is based on surface plasmon resonance as well as the high values at the sharp-boundary portion of the optical fiber probe. Now, the AFM probe tip and the PS nanoparticle were in the near-field region, and an obviously enhanced electric field appears in the gap between the metallic AFM probe tip and the PS nanoparticle. The surface plasmon resonance and the edge-enhancement phenomenon can affect the electric field distribution with the secondary enhancement phenomenon, presenting an electrical intensity as high as 3.6859 V/m underneath the metallic AFM probe tip. If the gap between the AFM probe tip and the PS nanoparticle is reduced, then a more pronounced near-field enhancement effect can be obtained for the nanospot-soldering operation. Because of the mutual influence of the surface plasmon and the positional relation between the optical fiber probe and the AFM probe, the near-field distribution was asymmetrical on the central axis of the optical fiber probe and the AFM probe. Observing the electric field distribution at the PS nanoparticle, the enhancement effect appears in the upper and the lower sides of PS nanoparticle as a result of the polarization direction of the incident laser; the laser can penetrate into the PS nanoparticle with high electric-field intensity.

As an electromagnetic wave, the laser has high energy, which is determined by the Poynting vector and is represented as

$$\mathbf{S} = \mathbf{E} \times \mathbf{H} \tag{1}$$

Here, **S** denotes the Poynting vector and **E** and **H** are the electric intensity and magnetic intensity, respectively.

According to classical electromagnetic theory, the electric field can be converted into the thermal field with the formula

$$Q = \frac{\omega_1}{8\pi}\varepsilon_t'' |\mathbf{E}|^2 \tag{2}$$

where $\omega_1$ is the frequency of incident laser, $\varepsilon_t''$ is the imaginary component of the relative permittivity of the AFM probe, and **E** is the electric field strength.

In addition, the magnetic intensity **H** can be replaced by the electric intensity **E**, on the basis of the Maxwell equations. Therefore, the size of the electromagnetic energy of the Poynting vector can be expressed as

$$I = S = 0.5c\varepsilon_0 n\mathbf{E}^2 \tag{3}$$

where $I$ is the light intensity, $c$ is the velocity of light, and $\varepsilon_0$ and $n$ indicate the dielectric constant of vacuum and the refractive index of the medium, respectively.

Thus, the electric field is converted into a thermal problem. Considering the near-field enhancement effect of an optical fiber probe laser that irradiates the AFM probe, the AFM tip, with Rayleigh length $R^* = \lambda/(2\pi)$ in the vertical direction, was applied with a light intensity of $1.9 \times 10^{10}$ W/m$^2$, and the thermal distribution of AFM probe was simulated, with the results shown in Figure 4. The AFM probe tip can achieve a

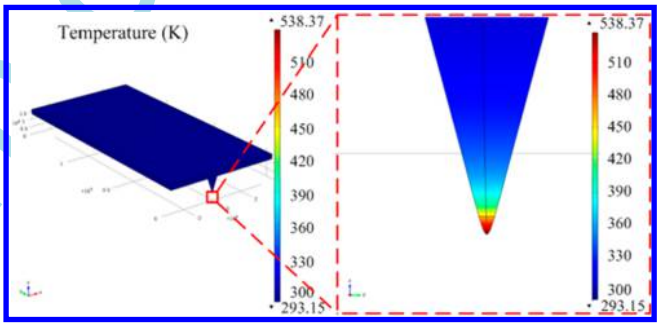


**Figure 4.** Thermal field distribution of the AFM probe tip irradiated by a laser with an input power of $1.9 \times 10^{10}$ W/m$^2$, achieving a stable temperature of the AFM tip on the basis of the near-field enhancement effect for nanosoldering.

temperature of 538.37 K, which is higher than the melting point of the PS nanoparticle. Thus, according to the theoretical analysis, the nanospot soldering of PS nanoparticles can be achieved; the nanospot soldering of PS nanoparticles was subsequently carried out.

## 4. EXPERIMENTS AND DISCUSSION

On the basis of the systemic diagram in Figure 1, we set up the experimental platform for nanospot soldering that is shown in Figure 5. The optical fiber probe (MF04, NT-MDT, Russia) was made of a single-mode tapered probe with an aperture diameter of 100 nm. Because it is an important component for laser input, the optical fiber probe can withstand the maximum laser power of 400 mW. Therefore, before the nanosoldering experiments and on the basis of its adjustable laser power, we selected the single-mode polarized laser instrument (Lumics LU0808M100, Connect Laser, China) with a maximum power of 64 mW for the incident laser source. The optical efficiency of optical fiber probe, with a diameter of 100 nm, is about $10^{-3}$. To provide a theoretical basis for nanospot-welding, assuming laser-input powers of 11 and 60 mW, the laser-output powers are 11 and 60 $\mu$W, respectively, at the exit of the optical fiber probe. According to eq 3




DOI: 10.1021/am506344j
ACS Appl. Mater. Interfaces 2015, 7, 2294−2300

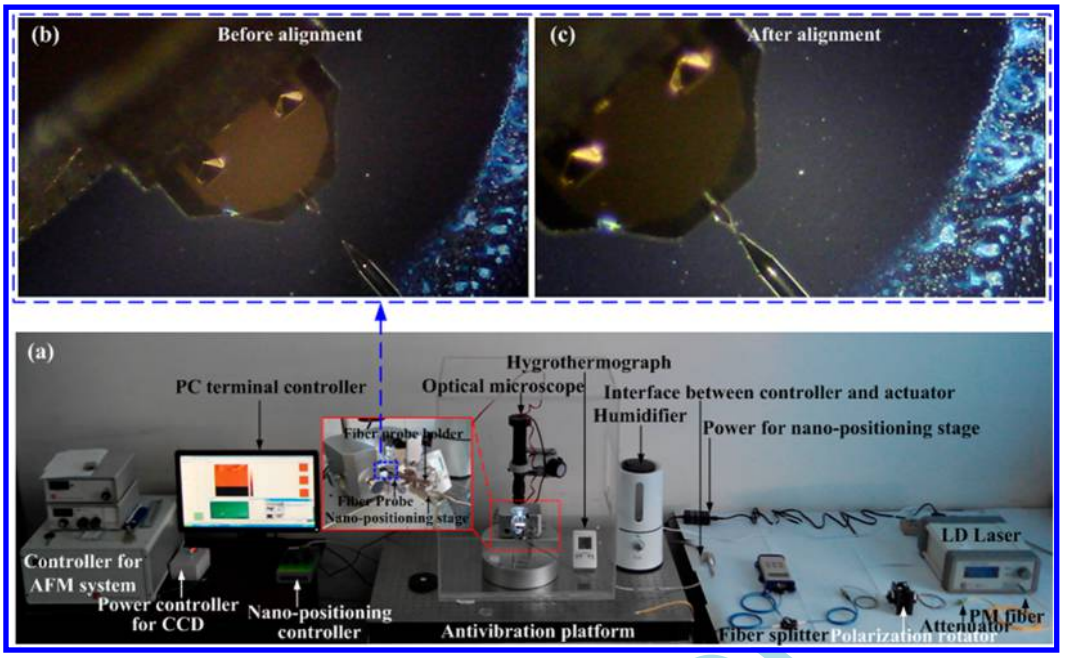


**Figure 5.** (a) Experimental platform for nanospot soldering of polystyrene nanoparticles. (b) Before and (c) after alignment between optical fiber probe and AFM probe tip.

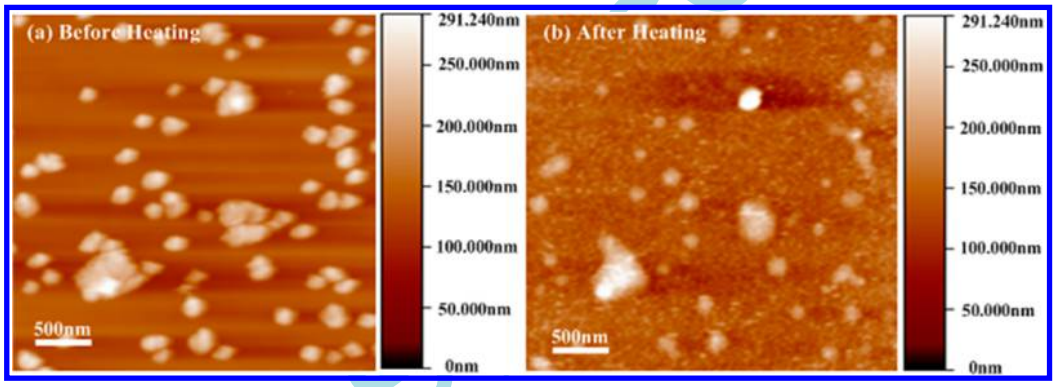


**Figure 6.** Soldering of polystyrene nanoparticles (a) before and (b) after heating with the thermal substrate.

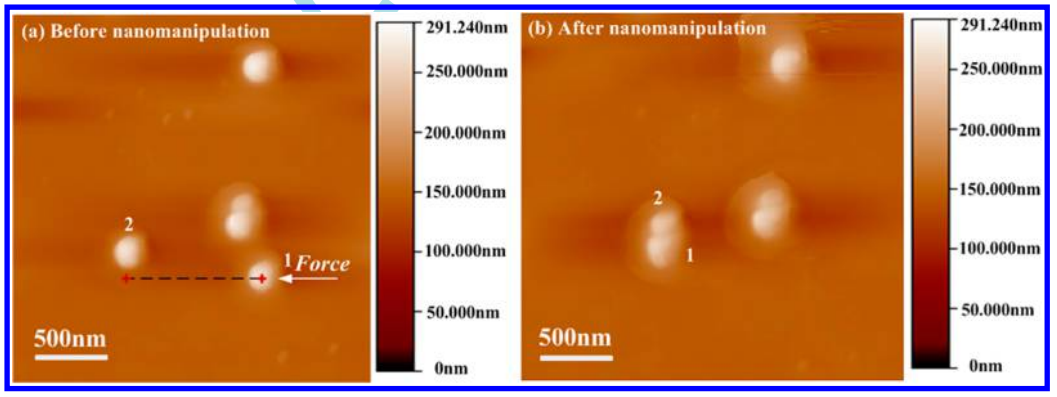


**Figure 7.** AFM images (a) before and (b) after nanomanipulation of 120 nm polystyrene particles that were based on the vector-scanning mode of the AFM system.

and the near-field enhancement effect, the light intensity applied to AFM probe tip is $1.9 \times 10^{10}$ and $1.04 \times 10^{11}$ W/m$^2$, respectively. Then, the corresponding simulations were carried out, obtaining stable temperatures of the AFM probe of 538.37 and 1197.5 K; these data provide theoretical guidance for nanospot-soldering experiments.

In addition, in order to allow adjustment of the distance between optical fiber probe and the AFM probe, the optical fiber probe was adhered to a metallic syringe needle that was attached to a 3D nanopositioning stage with an ultrahigh resolution of 1 nm (SLC-1720-s, SmarAct, Germany). In addition, the position of the sample was monitored in situ by AFM imaging on a reconstructive scanning probe microscope (SPM) platform (CSPM 5500, Being Nano-Intruments, China).


DOI: 10.1021/am506344j
ACS Appl. Mater. Interfaces 2015, 7, 2294−2300

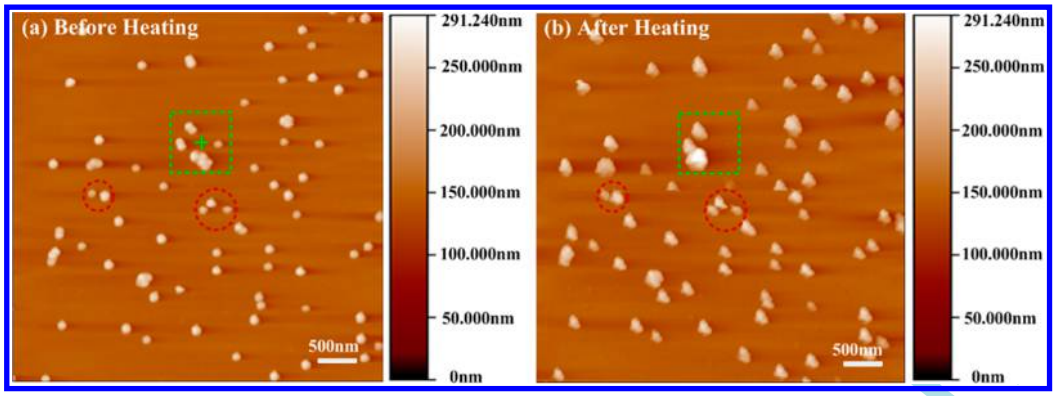


**Figure 8.** Nanospot soldering of polystyrene nanoparticles (a) before and (b) after heating with an optical-fiber-probe laser irradiating AFM probe tip (laser power = 60 mW).

To study nanospot soldering and show its advantages, we first conducted experiments focused on the soldering of PS nanoparticles with the thermal substrate. In the corresponding experiments, the heating execution unit, with a magnet at the bottom, was placed on top of the piezoelectric stage, keeping it in contact with the magnetic force. The dispersion solution of 120 nm PS nanoparticles, treated by an ultrasonic instrument, was used to coat the clean Si-substrate surface and dried with a flow of $N_2$. Then, the Si wafer with the PS nanoparticles was placed on the heating unit for scanning and imaging. By setting the temperature of the heating unit to 150 °C, the temperature is higher than the glass-transition temperature of the PS nanoparticles and is sufficient to achieve nanosoldering of the PS nanoparticles. In the experiments, a 3 min heating time was used for heating the PS nanoparticles. Thereafter, the heating unit and the Si substrate were cooled for 20 min to prevent position drift resulting from thermal expansion that occurred during scanning and imaging. The experimental results, before and after heating, are shown in Figure 6. Figure 6a reflects to some extent the information for a single particle. Figure 6b shows that adjacent nanoparticles formed larger mounds, as compared to Figure 6a. Thus, heating the whole substrate would result in the soldering of all of the nanosolders on the substrate, and it would not achieve nanospot soldering at the expected position. We mainly focused on the nanospot soldering with the new method.

Before nanospot soldering, nanomanipulation plays an important role in the fabrication of the PS nanostructure. To study the feasibility and accuracy of nanomanipulation, the PS nanoparticles were manipulated with the vector-scanning mode of the AFM system. Controlling the optimized parameters used in scanning and imaging, a large sample range was scanned for nano-objects, and then a more local, smaller range was scanned to produce clear images of the PS nanoparticles (Figure 7a). According to the specific vector used through the setting and conversion of coordinate values, the PS nanoparticle, marked as "1", was chosen as the nanomanipulation object and was manipulated by the propulsive force of the AFM probe tip. The nanomanipulation result is shown in Figure 7b, which illustrates that a nanoparticle can be artificially manipulated into a specified position and also demonstrates that vector-scanning-mode nanomanipulation is an effective method of nanomanipulation, providing an effective approach for carrying out nanospot soldering on adjacent nanoparticles.

For the nanospot-soldering experiments with PS nanoparticles, an alignment operation was first carried out between the optical fiber probe and the AFM probe via adjustment of the 3D nanopositioning stage and the angle of the optical fiber probe holder, which are shown in Figure 5. Simultaneously, in the height direction, the optical fiber probe was adjusted to irradiate the AFM probe tip and to ensure no contact with the substrate surface when the AFM system carries out scanning and imaging. Over the whole experiment, the taping mode was used for scanning and imaging. For nanosoldering, a gap of 2−5 nm was set between the optical fiber probe and the AFM probe tip under the noncontact mode. To achieve nanospot-soldering, the agminate PS nanoparticles, marked with the green square in Figure 8a, were chosen as the operation objects. The geometric center, marked with the green cross, became the location of the AFM probe tip that was heated by the optical fiber probe laser. In the nanospot-soldering process, the laser power and the duration time were set at 60 mW and 1 min, respectively, and the nanospot-soldering result is shown in Figure 8b. The PS nanoparticles near the thermal point of AFM probe tip were sintered into several mounds. In contrast, the nanoparticles that were far away from the hot spot still kept their monomer morphology (Figure 8b, red circles). This shows that nanospot soldering can be effectively achieved with an AFM probe that is irradiated by an optical fiber probe laser. However, after the nanospot heating process, the PS nanoparticle morphology had a deformation of a certain angularity without uniform roundness. According to the SEM images of the AFM probe tip morphology before and after nanosoldering (Figure 9), there is almost no modification of the

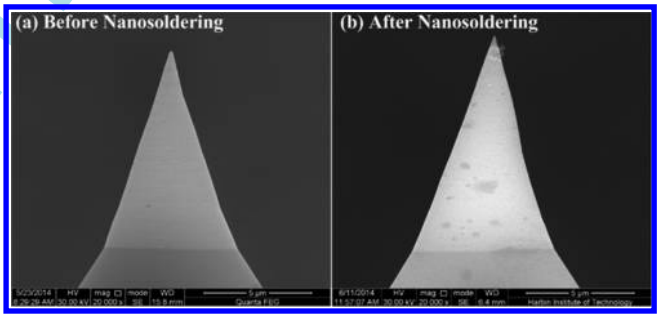


**Figure 9.** SEM images of AFM probe tip morphology (a) before and (b) after nanosoldering with an optical-fiber-probe laser irradiating the AFM probe tip.

AFM probe tip in the nanosoldering, scanning, and imaging operations under the higher temperature that is caused by the higher laser power. In addition, because the optical fiber probe laser could also illuminate the surrounding PS nanoparticles when it irradiated the AFM probe tip, the near-field enhancement effect on nanoparticles caused the generation of the deformation under the higher laser power, without the melting of nanoparticles and the merging together of the adjacent nanoparticles.

Considering that the higher laser power can affect the other surrounding PS nanoparticles, the nanospot soldering of PS nanoparticles was carried out in succession under the lower laser power (set to 11 mW in subsequent experiments). To clearly distinguish the deformation of nanoparticles, the scanning area was reduced from the original before nanospot soldering, and two adjacent PS nanoparticles were selected as the nanospot-soldering object in Figure 10a. For the nanospot-soldering effect, the AFM probe was positioned at the center position of the two adjacent nanoparticles (marked with the red crossing lines in Figure 10a). Changing the laser irradiation time to 5 min and keeping the other parameters constant,




DOI: 10.1021/am506344j
ACS Appl. Mater. Interfaces 2015, 7, 2294−2300

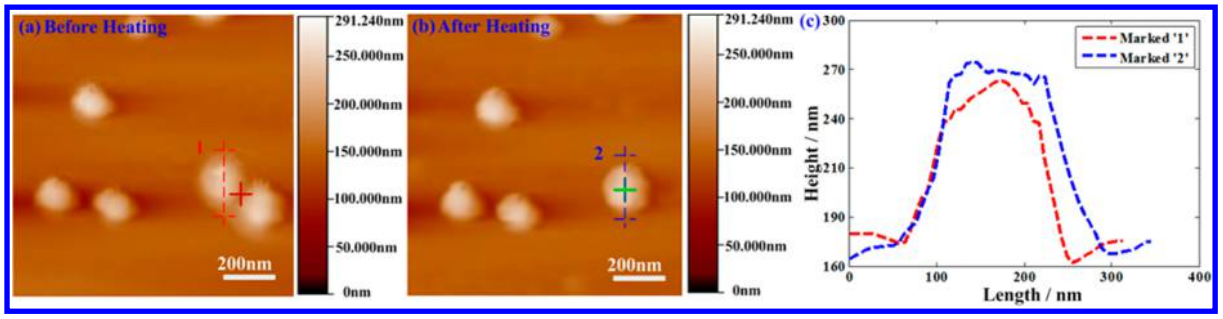


**Figure 10.** Nanospot-soldering process of polystyrene nanoparticles (a) before and (b) after heating operation with (c) the height topography throughout the process of the optical fiber probe laser irradiating the AFM probe tip (laser power = 11 mW).

the corresponding experiment was carried out in a manner that was similar to that of the above nanospot-soldering experiment. The nanospot-soldering result is shown in Figure 10b, which shows that after the melting, agglomerating, and cooling processes the two nanoparticles were sintered together well; they became a larger mound (green cross) that has good roundness, resulting from the surface-tension effect in the liquid state. The center position of the mound coincides exactly with the heating spot of the AFM probe tip that was irradiated by the laser (Figure 10a, red cross). In addition, the morphology of the surrounding PS nanoparticles has no apparent deformation or other effects. Therefore, the new method of an optical fiber probe laser that irradiates the AFM probe can effectively achieve the nanospot-soldering process without the damage caused by other nanosolders or nanodevices, which also provides a promising technical approach for the application of nanosoldering in nanoscience and nanotechnology.

## 5. CONCLUSIONS

The nanospot-soldering method that uses an optical fiber probe laser to irradiate the AFM probe, was proposed on the basis of the near-field enhancement effect. The electric and thermal field distributions were theoretically analyzed in simulations. The near-field enhancement effect can appear underneath the AFM probe tip, and it can cause the AFM probe tip achieve the high temperature necessary for nanospot soldering. During the soldering operation with the heating substrate, all of the polystyrene nanoparticles can be nanosoldered, and the adjacent nanoparticles can be sintered into larger mounds with the thermal substrate, which would not achieve nanospot soldering at the expected position. Using a nanomanipulation method, the polystyrene nanoparticles can be manipulated into the designated position. Then, the adjacent polystyrene nanoparticles can be sintered into a larger mound after the melting, agglomerating, and cooling of nanoparticles, which demonstrates that the method using an optical fiber probe laser to irradiate the AFM probe can effectively achieve the nanospot soldering of polystyrene nanoparticles and provides a promising technical approach for the application of nanosoldering in nanoscience and nanotechnology.

## ■ ASSOCIATED CONTENT

### Supporting Information

Thermal field distribution of the AFM probe tip that was irradiated by a laser with an input power of $1.04 \times 10^{11}$ W/m$^2$, temperature of the AFM probe tip that was irradiated by a laser with a different input power, and the nanospot-soldering process of polystyrene nanoparticles with an optical fiber probe laser irradiating the AFM probe (laser power = 11 mW). This material is available free of charge via the Internet at http://pubs.acs.org.

## ■ AUTHOR INFORMATION

### Corresponding Author

*Phone: +86 29 82663870. E-mail: cjlxjtu@mail.xjtu.edu.cn.

### Notes

The authors declare no competing financial interest.

## ■ ACKNOWLEDGMENTS

This project was supported by the China Postdoctoral Science Foundation (2014M562397); the State Key Laboratory of Surface Physics and Department of Physics, Fudan University (KF2014_04); the Research Support Program, Xi'an Jiaotong University, China (08142037); and the National Natural Science Foundation of China (51275122). All of the authors gratefully acknowledge their support.

## ■ REFERENCES

(1) Shulaker, M. M.; Hills, G.; Patil, N.; Wei, H.; Chen, H. Y.; Wong, H. S. P.; Mitra, S. Carbon Nantube Computer. *Nature* **2013**, *501*, 526−530.

(2) Xia, F. Graphene: Electrons en Masse. *Nat. Nanotechnol.* **2014**, *9*, 575−576.

(3) Joyce, H. J.; Gao, Q.; Hoe Tan, H.; Jagadish, C.; Kim, Y.; Zou, J.; Smith, L. M.; Jackson, H. E.; Yarrison-Rice, J. M.; Parkinson, P.; Johnston, M. B. III−V Semiconductor Nanowires for Optoelectronic Device Applications. *Prog. Quantum Electron.* **2011**, *35*, 23−75.

(4) Milani, S.; Baldelli Bombelli, F.; Pitek, A. S.; Dawson, K. A.; Rädler, J. Reversible versus Irreversible Binding of Transferrin to Polystyrene Nanoparticles: Soft and Hard Corona. *ACS Nano* **2012**, *6*, 2532−2541.

(5) Qi, X. Y.; Yan, D.; Jiang, Z.; Cao, Y. K.; Yu, Z. Z.; Yavari, F.; Koratkar, N. Enhanced Electrical Conductivity in Polystyrene Nanocomposites at Ultra-Low Graphene Content. *ACS Appl. Mater. Interfaces* **2011**, *3*, 3130−3133.

(6) Henke, P.; Lang, K.; Kubát, P.; Sýkora, J.; Šlouf, M.; Mosinger, J. Polystyrene Nanofiber Materials Modified with an Externally Bound Porphyrin Photosensitizer. *ACS Appl. Mater. Interfaces* **2013**, *5*, 3776−3783.

(7) Johnson, A. S.; Anderson, K. B.; Halpin, S. T.; Kirkpatrick, D. C.; Spence, D. M.; Martin, R. S. Integration of Multiple Components in Polystyrene-based Microfluidic Devices Part I: Fabrication and Characterization. *Analyst* **2013**, *138*, 129−136.

(8) Anderson, K. B.; Halpin, S. T.; Johnson, A. S.; Martin, R. S.; Spence, D. M. Integration of Multiple Components in Polystyrene-based Microfluidic Devices Part II: Cellular Analysis. *Analyst* **2013**, *138*, 137−143.

(9) Yun, D. J.; Hong, K.; Kim, S. H.; Yun, W. M.; Jang, J. Y.; Kwon, W. S.; Park, C. E.; Rhee, S. W. Multiwall Carbon Nanotube and Poly (3,4-Ethylenedioxythiophene): Polystyrene Sulfonate (PEDOT:PSS) Composite Films for Transistor and Inverter Devices. *ACS Appl. Mater. Interfaces* **2011**, *3*, 43−49.





DOI: 10.1021/am506344j
*ACS Appl. Mater. Interfaces* 2015, 7, 2294−2300

(10) Yi, D. K.; Seo, E.; Kim, D. Fabrication of a Mesoscale Wire: Sintering of a Polymer Colloid Arrayed Inside a One-Dimensional Groove Pattern. *Langmuir* **2002**, *18*, 5321−5323.
(11) Harel, E.; Meltzer, S. E.; Requicha, A. A. G.; Thompson, M. E.; Koel, B. E. Fabrication of Polystyrene Latex Nanostructures by Nanomanipulation and Thermal Processing. *Nano Lett.* **2005**, *5*, 2624−2629.
(12) Girard, C.; Dereux, A. Near-field Optics Theories. *Rep. Prog. Phys.* **1996**, *59*, 657.
(13) Sangu, S.; Kobayashi, K.; Ohtsu, M. Optical Near Fields as Photo-Matter Interacting Systems. *J. Microsc. (Oxford, U.K.)* **2001**, *202*, 279−285.
(14) Novotny, L.; Stranick, S. J. Near-field Optical Microscopy and Spectroscopy with Pointed Probes. *Annu. Rev. Phys. Chem.* **2006**, *57*, 303−331.
(15) Novotny, L.; Van Hulst, N. Antennas for Light. *Nat. Photonics* **2011**, *5*, 83−90.
(16) Palik, E. D., Ed. *Handbook of Optical Constants of Solids*, 7th ed.; Academic Press: Orlando, FL, 1985.





DOI: 10.1021/am506344j
*ACS Appl. Mater. Interfaces* 2015, 7, 2294−2300